[4] J. Glinianowicz, J. Jakuse, S. Szczepanski, and Y. Sun, "High-frequency two-input CMOS OTA for continuous time filter applications," *Proc. Inst. Electr. Eng. Circuits, Devices Syst.*, vol. 147, no. 1, pp. 13–18, 2000.
[5] A. Wyszynski, "Low-voltage CMOS and BiCMOS triode transconductors and integrators with gain-enhanced linearity and output impedance," *Electron. Lett.*, vol. 30, no. 3, pp. 211–213, 1994.
[6] S. O. Lee, S. B. Park, and K. R. Lee, "New CMOS triode transconductor," *Electron. Lett.*, vol. 30, no. 12, pp. 946–948, 1994.
[7] N. P. J. Greer and P. B. Denyer, "New folded cascode transconductor for bandpass ladder filter," *Proc. Inst. Electr. Eng*, pt. G, vol. 138, no. 5, pp. 551–556, 1991.
[8] A. L. Coban and P. E. Allen, "Low-voltage CMOS transconductance cell based on parallel operation of triode and saturation transconductors," *Electron. Lett.*, vol. 30, no. 14, pp. 1124–1126, 1994.
[9] B. Stefanelli and A. Kaiser, "A 2-μm CMOS fifth-order low-pass continuous-time filter for video-frequency applications," *IEEE J. Solid-State Circuits*, vol. 28, no. 7, pp. 713–718, July 1993.
[10] Q. Huang, "A MOSFET-only continuous-time bandpass filter," *IEEE J. Solid-State Circuits*, vol. 32, no. 2, pp. 147–158, Feb. 1997.
[11] E. A. M. Klumperink, C. H. J. Mensink, and P. M. Stroet, "Comment: Low-voltage CMOS transconductance cell based on parallel operation of triode and saturation transconductors," *Electron. Lett.*, vol. 30, no. 22, pp. 1824–1825, 1994.
[12] J. Mahattanakul and C. Toumazou, "Tunable low-distortion BiCMOS transconductance amplifier," *Electron. Lett.*, vol. 34, no. 2, pp. 175–176, 1998.

Fifth-Order State-Space Modeling of Class E Amplifiers with Finite-Series Inductance and an Anti-Parallel Diode at the Switch

Lien Seng Tan, David G. H. Tan, Richard A. McMahon, and Douglas R. H. Carter

***Abstract*—A state-space model is developed to enable a general analysis of the class E amplifier with a power-MOSFET switch under nonoptimal and optimal conditions. That is, it permits analysis of nonzero voltage switching and nonzero current switching operation, as well as the optimal zero voltage switching (ZVS) and zero current switching (ZCS) condition. This is achieved by improving the representation of the power MOSFET switch by the inclusion of a series inductance, a model for the on-state resistance and switching time, and a model for the anti-parallel body diode. An optimal 100-kHz class E amplifier was designed and constructed, using the model to choose component values. Experimental results show good agreement with the predictions of the state-space model for both optimal and nonoptimal operating conditions.**

***Index Terms*—Class-E amplifier, high frequency, power conversion, state-space analysis.**

I. Introduction

The class-E amplifier, first proposed by Sokal and Sokal [1], [2], is a resonant switch-mode circuit. Switching losses are eliminated in the optimum operating conditions of zero voltage switching (ZVS) and zero current switching (ZCS) at turn on. The class E amplifier is therefore a prime candidate for efficient operation at high switching frequencies. The circuit is simple, typically using one switch coupled to a resonant network as shown in Fig. 1. However, the interaction of the resonant network, the supply choke L_1 and the continuously operated switch makes operation at the optimum conditions sensitive to component values.

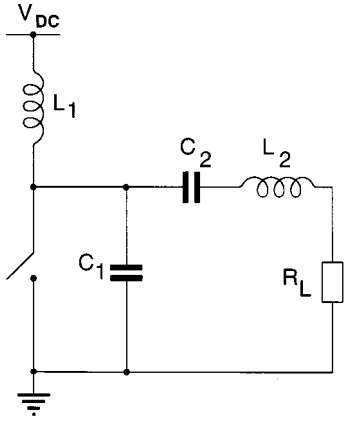

Fig. 1. Schematic of the basic class E amplifier.

Early attempts to analyze the class E amplifier made certain assumptions in order to derive approximate analytical solutions to the basic fourth order governing [3]–[6]. The most common assumptions were that L_1 is large enough to maintain a constant supply current, that the quality factor, Q_L, of the resonant load is high enough to assume a sinusoidal output current and that the switch is ideal. However, due to the sensitivity of the circuit, these assumptions lead to significant errors in the predicted performance.

More recently, numerical methods have been proposed by Mandojana *et al.* [7] and Avratoglou *et al.* [8]. These methods avoid the need for the above mentioned assumptions. However, other assumptions are made which do not allow accurate prediction of circuit behavior under non-ZVS and non-ZCS conditions. Therefore, these models are unsuitable for a general investigation of the circuit, because in practise a class E amplifier rarely operates under optimal conditions at all times due to the inevitable variation of load impedance, the tolerances of component values and their variation over time and temperature.

The work presented in this paper extends the state-space approach of Mandojana *et al.* to allow accurate prediction of performance under nonoptimal conditions, i.e., without ZVS and ZCS. The fifth-order state-space model presented in Section II includes inductance in series with the switch, L_s, which affects circuit behavior when there is a positive voltage across the switch at turn on. Its effect is also important at high switching frequencies. The algorithm used in the model includes the effect of the anti-parallel diode present across the switch when a power MOSFET is used. Its inclusion enables accurate prediction of circuit behavior under nonideal operating conditions. To take account of the nonzero duration of power MOSFET switching times, which are significant at multimegahertz switching frequencies, the switch is modeled as a time-dependent resistance with transition regions between the on and off states. The fifth-order model enables accurate prediction of the performance of the class E amplifier under any operating conditions—optimum or otherwise.

The model has been used in a design example (Section III) to choose component values for optimum operation and an experimental circuit has been constructed to this design in order to verify the accuracy of the

Manuscript received April 22, 1998; revised April 23, 2001. This work was supported in part by the Engineering and Physical Science Research Council (U.K), under Grant GR/J87237. The work of L. S. Tan was supported in part by the Cambridge Commonwealth Trust and in part Blue Circle Industries. This paper was recommended by Associate Editor K. Roy.

L. S. Tan, R. A. McMahon, and D. R. H. Carter are with the Department of Engineering, University of Cambridge, Cambridge CB2 1PZ, U.K.

D. G. H. Tan was with the Department of Applied Mathematics and Theoretical Physics, University of Cambridge, Cambridge CB3 9EW, UK. He is now with the Department of Mathematics and Statistics, University of Otago, Dunedin, New Zealand.

Publisher Item Identifier S 1057-7122(01)07718-2.

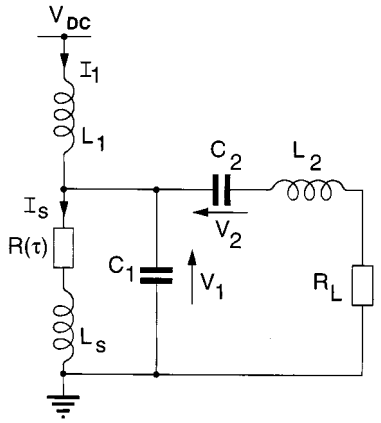

Fig. 2. Model used for numerical simulation of the class E amplifier.

model (Section IV). Further comparisons are made between the model and experimental circuit under nonoptimum conditions, showing the simulation results to be in close agreement with the experimental measurements.

II. Circuit Analysis

The circuit used in our model of the class E amplifier is shown in Fig. 2. The switch resistance varies with time τ and is denoted by $R(\tau)$. The switch inductance L_s is a composite inductance that represents the combined inductance of the bond wires connecting the die of the semiconductor switch to its package and the stray inductance of external wiring. Kirchoff's voltage and current laws applied to the circuit yield the system of differential equations

$$L_1\frac{dI_1(\tau)}{d\tau}+V_1(\tau)= V_{DC} \tag{1}$$

$$C_1\frac{dV_1(\tau)}{d\tau}+C_2\frac{dV_2(\tau)}{d\tau}+I_s(\tau)-I_1(\tau)= 0 \tag{2}$$

$$L_2C_2\frac{d^2V_2(\tau)}{d\tau^2}+R_LC_2\frac{dV_2(\tau)}{d\tau}+V_2(\tau)-V_1(\tau)= 0 \tag{3}$$

$$L_s\frac{dI_s(\tau)}{d\tau}+I_s(\tau)R(\tau)-V_1(\tau)= 0. \tag{4}$$

The period of the switch is denoted by T and the dimensionless time, t is defined as

$$t=\frac{\tau}{T} \tag{5}$$

and the dimensionless state vector

$$\begin{aligned}\underline{x}(t)&=[x_1(t),x_2(t),x_3(t),x_4(t),x_5(t)]^T\\&=\left[\frac{L_1I_1(\tau)}{V_{DC}T},\frac{V_1(\tau)}{V_{DC}},\frac{V_2(\tau)}{V_{DC}},\dot{x}_3(t),\frac{L_sI_s(\tau)}{V_{DC}T}\right]^T\end{aligned} \tag{6}$$

where $\dot{x}$ means dx/dt and $\underline{x}^T$ means the transpose of the vector $\underline{x}$. The system (1)–(4) rewritten in terms of the dimensionless state vector yields the state equations

$$\dot{\underline{x}}(t)=A(t)\underline{x}(t)+\underline{u} \tag{7}$$

where

$$A(t)=\begin{bmatrix}0 & -1 & 0 & 0 & 0\\ \frac{T^2}{L_1C_1} & 0 & 0 & -\frac{C_2}{C_1} & -\frac{T^2}{L_sC_1}\\ 0 & 0 & 0 & 1 & 0\\ 0 & \frac{T^2}{L_2C_2} & \frac{-T^2}{L_2C_2} & -\frac{TR_L}{L_2} & 0\\ 0 & 1 & 0 & 0 & -\frac{T\hat{R}(t)}{L_s}\end{bmatrix} \tag{8}$$

$$\underline{u}=[1\ 0\ 0\ 0\ 0]^T \tag{9}$$

and

$$\hat{R}(t)\equiv R(\tau). \tag{10}$$

The state variables $x_i(t)$ remain continuous provided that $\hat{R}(t)$ is always finite.

A. Periodic Solution

We first establish a simple result regarding the unforced system (also known as the short-circuited system) where V_{DC} is zero. Suppose that initially the capacitors and inductors of the circuit contain some energy and that the system is unforced. The corresponding state vector of this unforced system, which we denote by $\underline{y}(t)$, is, therefore, governed by

$$\dot{\underline{y}}(t)=A(t)\underline{y}(t). \tag{11}$$

Not surprisingly, the energy in the unforced system is progressively dissipated and the state vector tends to the zero vector. To see that this is the case, we consider the system energy normalized by the factor $C_2V_{DC}^2$, defined as

$$E_y(t)=\frac{1}{2}\left[\frac{T^2}{L_1C_2}y_1^2+\frac{C_1}{C_2}y_2^2+y_3^2+\frac{C_2L_2}{T^2}y_4^2+\frac{T^2}{L_sC_2}y_5^2\right]. \tag{12}$$

Then differentiation of (12) together with (11) and (8) shows that the rate of change of energy is

$$\begin{aligned}\dot{E}_y(t)&=\frac{T}{C_2V_{DC}^2}\left[-R_L\left(\frac{C_2V_{DC}}{T}\right)^2y_4^2-\hat{R}(t)\left(\frac{V_{DC}T}{L_s}\right)^2y_5^2\right]\\&=-\frac{R_LC_2}{T}y_4^2-\frac{\hat{R}(t)T^3}{C_2L_s^2}y_5^2.\end{aligned} \tag{13}$$

Equation (13) is a mathematical statement of the physical property of the circuit that energy is dissipated by $\hat{R}(t)$ and R_L. Because the rate of change of energy is always negative, the system energy tends to zero and hence the state vector for the unforced system also tends to zero, i.e., $\lim_{t\to\infty}E_y(t)=0,\Rightarrow\lim_{t\to\infty}\underline{y}(t)=\underline{0}$.

It follows immediately that the forced system (7) ultimately attains periodic behavior, irrespective of the initial conditions, assuming only that the switch is periodic with period T. Expressed in our dimensionless variables, the periodicity condition is that

$$A(t)=A(t+1). \tag{14}$$

Attainment of periodic behavior follows because the energy-dissipation argument applies to $\underline{y}(t)=\underline{x}(t+n)-\underline{x}(t)$, for any integer n, i.e., to the difference between the forced system state vector and the same state vector time-shifted by an integer number of periods. That the forced system attains periodicity irrespective of the initial conditions, follows because the energ-dissipation argument can also be applied to $\hat{\underline{y}}(t)=\hat{\underline{x}}(t)-\underline{x}(t)$, where $\hat{\underline{x}}(t)$ is any other solution arising from different initial conditions. These results are true provided only that $A(t)$ has period 1, i.e., $\hat{R}(t)$ has period T. In particular, nonzero rise and fall times of $\hat{R}(t)$ can be accommodated in the analysis provided that $\hat{R}(t)$ is continuous.

The results of this section are not at all surprising but we feel it is useful to establish clearly the assumptions necessary to ensure periodic behavior. Note that this does not mean the state variables/waveforms are restricted to a single frequency. Higher harmonics are compatible with periodicity, with the implication that Q_L can be finite.

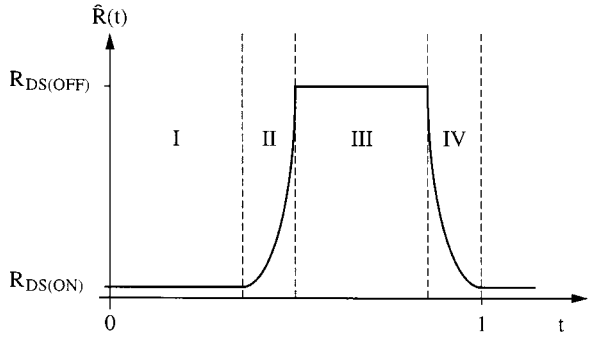

Fig. 3. Variation of the switch resistance, $\hat{R}(t)$, during one period showing the four distinct phases of operation.

B. Representation of the Periodic Solution

The periodic solution of (7) can be expressed in the form

$$\underline{x}(t) = \underline{x}_P(t) + M(t)\underline{\alpha} \tag{15}$$

where $\underline{x}_P(t)$ and $M(t)\underline{\alpha}$ denote a particular integral and complementary function respectively. Equation (7) is satisfied by (15), provided that the 5 by 5 matrix $M(t)$ and 5 by 1 vector $\underline{x}_P(t)$ satisfy

$$\dot{M}(t) = A(t)M(t) \tag{16}$$

$$\dot{\underline{x}}_P(t) = A(t)\underline{x}_P(t) + \underline{u}. \tag{17}$$

For the sake of definiteness, the following initial conditions were chosen:

$$M(0) = I \tag{18}$$

$$\underline{x}_P(0) = \underline{0}. \tag{19}$$

The condition for periodicity is

$$\underline{x}(0) = \underline{x}(1). \tag{20}$$

Equations (15), (18)–(20) imply that the periodic solution has

$$\begin{aligned}\underline{\alpha} &= [M(0) - M(1)]^{-1}\,\underline{x}_P(1) \\ &= [I - M(1)]^{-1}\,\underline{x}_P(1).\end{aligned} \tag{21}$$

C. Numerical Implementation

To determine $M(t)$ and $\underline{x}_P(t)$ numerically, we solve (16) and (17) subject to (18) and (19) using a second-order implicit time-stepping scheme [9]. The differential equations are numerically stiff when the switch resistance is in the off state, so the implicit scheme was chosen because it ensures numerical stability. Our particular implementation was written in MATLAB (by The MathWorks, Inc. 24 Prime Park Way, Natick, MA 01760–1500). The numerical solutions of (16) and (17) are required only for a single period of the switch operation.

In the calculations presented in this paper, the period of the switch is normalized to unity. Rise and fall times of the switch are explicitly taken into account by dividing the switch resistance $\hat{R}(t)$ into four phases (see Fig. 3):

- Phase I: MOSFET on, $\hat{R}(t) = R_{\mathrm{DS(ON)}}$, duration t_{on}.
- Phase II: MOSFET turning off, $\hat{R}(t)$ rises from $R_{\mathrm{DS(ON)}}$ to $R_{\mathrm{DS(OFF)}}$, duration t_{rise}.
- Phase III: MOSFET off, $\hat{R}(t) = R_{\mathrm{DS(OFF)}}$, duration t_{off}.
- Phase IV: MOSFET turning on, $\hat{R}(t)$ falls from $R_{\mathrm{DS(OFF)}}$ to $R_{\mathrm{DS(ON)}}$, duration t_{fall}.

Note that

$$t_{\mathrm{on}} + t_{\mathrm{rise}} + t_{\mathrm{off}} + t_{\mathrm{fall}} = 1 \tag{22}$$

and the duty of the switch, ρ, is defined as

$$\rho = t_{\mathrm{on}} + 0.5(t_{\mathrm{rise}} + t_{\mathrm{fall}}). \tag{23}$$

The numerical model is not limited to predicting the performance of a class E amplifier with particular component values—it can also be used to find component values that give optimal circuit performance.

III. Design Example

In the class E amplifier, the values of L_1, L_2, C_1, C_2 and R_L for optimal operation are inter-dependent. However, the values of R_L, L_1 and L_2 are not critical and practical design considerations yield values for these components, leaving only C_1 and C_2 to be found.

The class E amplifier is said to be operating optimally [1] when the voltage across the switch and the rate of change of this voltage are both equal to zero at the moment the switch starts to turn on ($t_{\mathrm{turn\ on}} = 1 - t_{\mathrm{fall}}$). However, these conditions can be relaxed to reflect the tolerance of the practical circuit to slightly nonoptimal operation, giving the following constraints

$$\begin{aligned} V_{1(\mathrm{turn\ on})} &\equiv V_1(\tau)\Big|_{\tau = T t_{\mathrm{turn\ on}}} \le V_{1(\mathrm{lim})} \\ V'_{1(\mathrm{turn\ on})} &\equiv \frac{dV_1(\tau)}{d\tau}\Big|_{\tau = T t_{\mathrm{turn\ on}}} \le V'_{1(\mathrm{lim})}. \end{aligned} \tag{24}$$

Given values of C_1 and C_2, $V_{1(\mathrm{turn\ on})}$ and $V'_{1(\mathrm{turn\ on})}$ are inferred straightforwardly from the state variables, as indeed are all other circuit quantities.

To verify the numerical model and demonstrate its use in choosing component values for optimal operation, a class E amplifier was designed for a load resistance of 70 Ω, switching frequency 100 kHz and supply voltage of 20 V. A IRF730 power MOSFET with 1 Ω on-state resistance was used as the switching device. The source inductance in the circuit, L_s comprising power MOSFET package inductance and circuit stray inductance, was estimated using resonance measurements to be 40 nH.

The off-state resistance of the power MOSFET was set to 100 MΩ. The power MOSFET was driven by a high speed gate driver that was capable of channel switching times of less than 10 ns, giving values for t_{rise} and t_{fall} of 0.001. With such fast switching times, the turn on and turn off transitions have very little effect on the circuit operation and the form of $\hat{R}(t)$ during these periods is unimportant—here a second order polynomial was used. The duty cycle of the power MOSFET was set to 50%, a value which generally gives the best device utilization [4], [10].

The class E amplifier will operate with a wide range of values for the supply inductor, L_1 [8]. Smaller values lead to increased output power at the expense of increased supply current ripple, and make it easier to keep the self-resonant frequency well above the switching frequency. However, circuit operation can only be sustained when L_1 exceeds a certain critical inductance given by $L_{1(\mathrm{crit})} = R_L/4\pi f$, which is 55.7 μH for the circuit considered here. A relatively large value of 1.5 mH has been used here to give low current ripple.

The value of the loaded quality factor, Q_L, given by

$$Q_L = \frac{2\pi f L_2}{R_L} \tag{25}$$

is a compromise. Increasing Q_L reduces the harmonic content of the load current, but requires more precise and stable tuning of the resonant

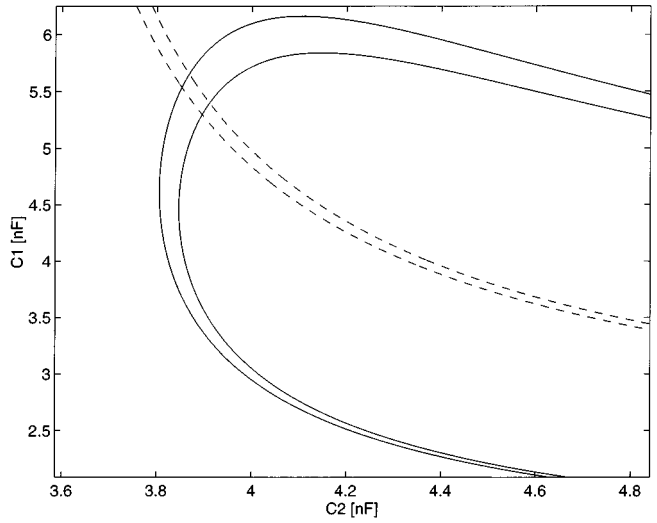

Fig. 4. Loci for the optimal class E amplifier designed in Section III with $L_s = 40$ nH. The solid lines border the region where $\left|V_{1(\text{turn on})}\right| \leq 1$ V, the dashed lines enclose the region where $\left|V'_{1(\text{turn on})}\right| \leq 0.5$ V/μs.

network. In addition, the increased voltages across C_2 and L_2 require expensive components with higher working voltages. In this design, 775 μH was used to give a quality factor of seven.

Fig. 4 shows the regions that satisfy constraints (24) with $V_{1(\text{lim})} = 1$ V (between solid lines) and $V'_{1(\text{lim})} = 0.5$ Vμ·s (between dashed lines) in the C_1-C_2 plane. The figure indicates that there is an intersection region where both conditions are satisfied, i.e., where optimal operation is achieved. In this design example, values of $C_1 = 5.48$ nF and $C_2 = 3.88$ nF from the intersection region were selected for experimental realization. The chosen values of $V_{1(\text{lim})}$ and $V'_{1(\text{lim})}$ specify the values of C_1 and C_2 for optimal operation to a tolerance of 1%.

IV. Model Verification

The above design was practically implemented. Both C_1 and C_2 included a variable capacitor element to enable tuning of the values. The capacitance C_1 was measured *in situ* on the circuit board to include the output capacitance of the IRF730 power MOSFET and circuit board stray capacitances. With the model-derived component values, the class E amplifier operated near to, but not at ZVS-ZCS conditions. This is expected because of the difficulty in the precise measurement of component values and the sensitivity of the class E amplifier to component values.

To make a direct comparison between the model and bench circuits, the values of C_1 and C_2 were tuned to give ZVS-ZCS conditions. The tuning process was carried out to null the uncertainties in the capacitor values based only on the ZVS-ZCS criterion. The measured values after tuning were 5.27 and 3.93 nF, respectively—an adjustment of less than 4% which is within the limits of impedance measurement error. A comparison of other measures of circuit behavior, given in Table I, shows that the model has good correlation with the bench circuit on all other parameters after the nulling procedure. Fig. 5 shows the simulated and bench waveforms for V_1 and I_s. This demonstrates that, taking into account measurement uncertainties, the model can provide accurate component values for optimal operation. By comparison, the Sokal equations yield values of C_1 and C_2 which are in error by up to 20% compared to the optimal values.

A. Effect of L_s

At the switching frequency of 100 kHz considered here, the impedance of the 40-nH source inductance is very small compared to other circuit impedances and has a small effect on the operating conditions of the class E amplifier. Surprisingly, the values of C_1 and C_2 for optimal operation change by only 7% when L_s is increased even to 40 μH.

Nonetheless, an increase to just 400 nH of source inductance, which does not greatly affect component values for optimal operation, does have a visible effect on the waveforms of the experimental class E amplifier. The switch waveforms, in Fig. 6, show oscillations in I_s following turn on. This is caused by a resonance between L_s and C_1, damped by the MOSFET on-state resistance, $R_{\text{DS(on)}}$, and which is excited by the start of current flow in the switch. The oscillations are accurately predicted by the fifth-order model simulations, which are also shown in Fig. 6. The values of C_1 and C_2 that give optimal operation are 5.46 and 3.87 nF, respectively, for 400 nH of source inductance. These capacitors were again tuned in the experimental setup to give ZVS-ZCS operation, and, as before, the required adjustment was less than the measurement uncertainty. Table I summarizes the operating parameters and shows good agreement between simulation and experiment.

The effect of L_s in the above example is quite benign because the damping effect of $\hat{R}(t)$ is quite strong and the resonant frequency is much higher than the switching frequency. However, at switching frequencies in the megahertz range the effect of switch-current oscillations will be significant on circuit operation and inclusion of the source inductance in the model is important.

Two cases of nonoptimal operation are now considered in order to illustrate the agreement between the fifth-order model and experimental results under nonoptimal conditions. The first case involves a positive value of $V_{1(\text{turn on})}$ and leads to a hard switched turn on of the power MOSFET. The second involves a negative value of $V_{1(\text{turn on})}$, resulting in conduction of the body diode of the power MOSFET. These two cases are examined by detuning the optimal class E amplifier with nonoptimal load resistances.

B. Nonoptimal Operation With Positive $V_{1(\text{turn on})}$

With an increase in the load resistance to 100 Ω the ZVS condition is not achieved, with V_1 measured to be 16 V at turn on, as shown in Fig. 7. This leads to the 4.6-A current transient observed in the power MOSFET's drain current as it rapidly discharges C_1. The drain current is also observed to continue as a damped oscillation at 10.7 MHz.

The effect of L_s is important in the operation of the circuit under these conditions. Previous analyses and numerical models ignored any inductance in series with the switch. Such a model would predict a transient amplitude of

$$\frac{V_{1(\text{turn on})}}{R_{\text{DS(on)}}} = \frac{16\text{ V}}{1\ \Omega} = 16\text{ A} \tag{26}$$

followed by an exponential decay. This predicted transient amplitude is over three times greater than the measured value.

By including L_s in the model, the amplitude of the transient is limited by the impedance it adds to the discharge path. Fig. 7 shows the simulated waveforms for $L_s = 40$ nH. The predicted current transient of 4.1 A is in good agreement with the measured value. The improved model also predicts the damped oscillation, arising from the second-order network L_s, C_1 and $\hat{R}(t)$. Various other parameters of class E amplifier performance are listed in Table II and show good agreement with experimental results.

TABLE I
COMPARISON OF PREDICTED AND EXPERIMENTAL PERFORMANCE PARAMETERS FOR OPTIMUM CONDITIONS WITH $L_s = 40$ AND 400 NH

	$L_s = 40$ nH			$L_s = 400$ nH		
	Simulation	Experiment	Error [%]	Simulation	Experiment	Error [%]
$I_{1(ave)}$ [A]	0.175	0.175	0.0	0.177	0.18	1.6
$I_{s(max)}$ [A]	0.482	0.465	3.6	0.488	0.47	3.9
$V_{1(max)}$ [V]	71.57	71.9	0.5	71.68	71.3	0.5
$V_{1(max)}/V_{DC}$	3.579	3.577	0.1	3.584	3.565	0.5
$V_{2(p-p)}$ [V]	256.2	255	0.5	258.6	262	1.3
P_{out} [W]	3.414	3.40	0.3	3.460	3.47	0.3
η [%]	97.95	97.1	0.7	97.86	96.4	0.7

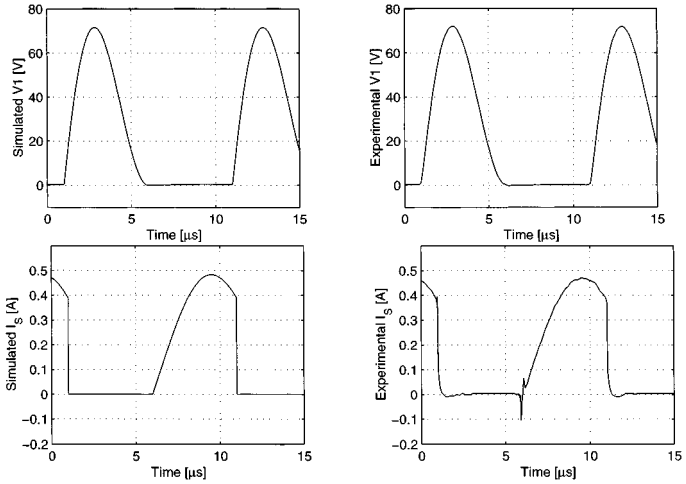

Fig. 5. Simulated and experimental waveforms of V_1 and I_s under optimal conditions with $L_s = 40$ nH . The turn on transient in the experimental I_s is current injected through the power MOSFET C_{GD} from the gate-drive circuit.

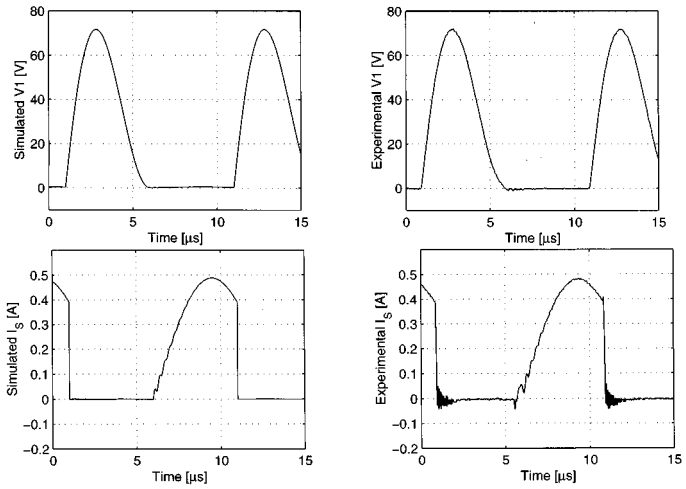

Fig. 6. Simulated and experimental waveforms of V_1 and I_s under optimal conditions with $L_s = 400$ nH.

Further improvements in the prediction accuracy of the model could be made by including the effect of the gate driver and the input and reverse transfer capacitances of the power MOSFET, and by considering the effect of the drain and source inductances of the power MOSFET separately. However, this would add considerably to the complexity of the model while only adding marginally to the accuracy improvement afforded by the inclusion of L_s alone.

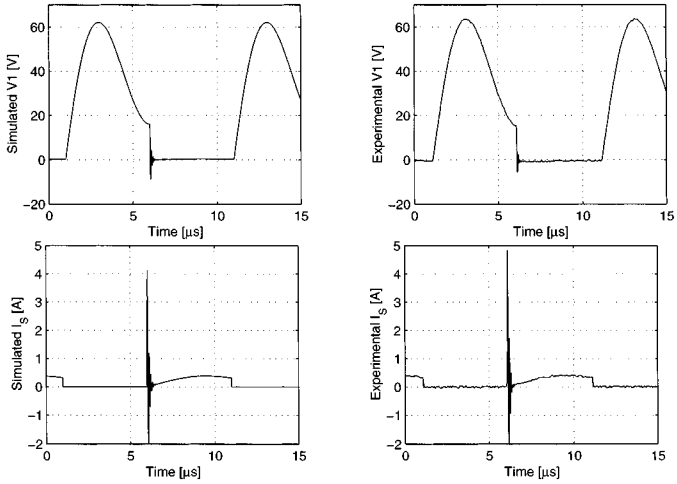

Fig. 7. Simulated and experimental waveforms of V_1 and I_s for $R_L = 100\ \Omega$.

TABLE II
COMPARISON OF PREDICTED AND EXPERIMENTAL PERFORMANCE PARAMETERS FOR NON-OPTIMAL CONDITIONS WITH $R_L = 100\ \Omega$.

	Simulation	Experiment	Error [%]
$I_{1(ave)}$ [A]	0.149	0.153	2.7
$I_{s(max)}$ [A]	4.126	4.50	9.1
$V_{1(turn\ on)}$ [V]	16.1	16	0.6
$V_{1(max)}$ [V]	62.2	62.3	0.2
$V_{1(max)}/V_{DC}$	3.11	3.13	0.6
$V_{2(p-p)}$ [V]	195.4	200	2.3
P_{out} [W]	2.854	2.98	4.4
η [%]	96.07	96.1	0.03

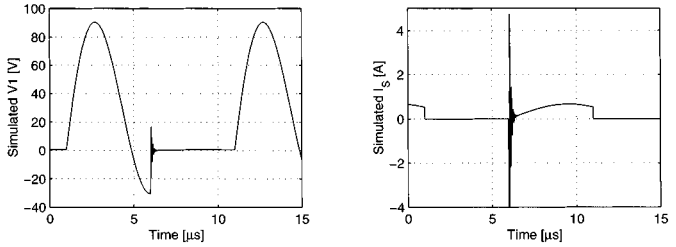

Fig. 8. Simulated waveforms of V_1 and I_s for $R_L = 40\ \Omega$ assuming no anti-parallel body diode.

C. Nonoptimal Operation with Negative $V_{1(\mathrm{turn\ on})}$

A decrease in the load resistance from its optimum value increases the quality factor of the load and tends to make V_1 swing to below the ground potential and yield a negative value for $V_{1(\mathrm{turn\ on})}$. However, in a class E amplifier that uses a power MOSFET for the switch, the integral body diode clamps negative-voltage excursions. This behavior

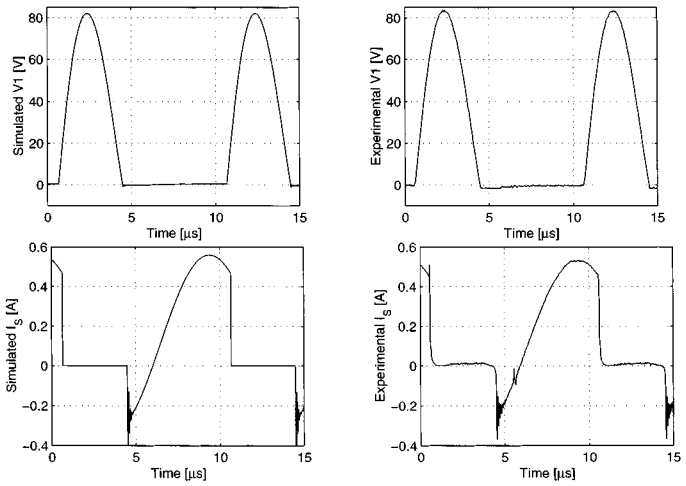

Fig. 9. Simulated and experimental waveforms of V_1 and I_s for $R_L = 40 \sim \Omega$ with duty modified to account for body diode of MOSFET. The turn–on transient in the experimental I_s is current injected through the power MOSFET C_{GD} from the gate drive circuit.

TABLE III
COMPARISON OF PREDICTED AND EXPERIMENTAL PERFORMANCE PARAMETERS FOR NON-OPTIMAL CONDITIONS WITH $R_L = 40\ \Omega$

	Simulation	Experiment	Error [%]
$I_{1(ave)}$ [A]	0.162	0.16	1.2
$I_{s(max)}$ [A]	0.560	0.54	3.6
$V_{1(max)}$ [V]	82.1	83.0	1.1
$V_{1(max)}/V_{DC}$	4.105	4.15	0.1
$V_{2(p-p)}$ [V]	325.8	326	0.2
P_{out} [W]	3.154	3.19	1.1
η [%]	97.1	97.0	0.1

was modeled by modifying the duty of the switch as described next, whilst retaining unaltered the governing state-space equations.

To demonstrate the problem, the load resistance was reduced to 40 Ω. Without allowing for the action of the body diode, the model predicts the waveforms shown in Fig. 8, $V_{1(\text{turn on})}$ of -15 V, and a reduced efficiency of 91.9%.

In a practical circuit, the power MOSFET body diode begins to conduct when the forward voltage across it reaches $V_F \approx 0.7$ V, the diode forward voltage, i.e., when $V_1 = -V_F$. It turns off when $I_s = 0$ A. At that instant ZVS-ZCS conditions exist across the power MOSFET and it is turned on. Therefore, there is a conduction path through the switch from the time the diode turns on until the power MOSFET turns off. Rather than introduce a diode into the model, this conduction path can be modeled using only $R_{\text{DS(ON)}}$ of the conducting power MOSFET. The model algorithm was modified to turn on the switch when $V_1 = -V_F$, effectively increasing the duty of the switch.

The switch voltage and current waveforms predicted by this modified algorithm are shown in Fig. 9, and demonstrate the increase of the switch duty to take account of the body diode conduction. The waveforms show good agreement with those observed experimentally (also shown in Fig. 9), in contrast to those that do not allow for the body diode (Fig. 8). Table III compares the performance parameters for the modified algorithm and experimental setup, once again showing that the model is in good agreement with experiment. Notably, the predicted efficiency of 97.1% is much closer to the measured efficiency of 97.0% than with the unmodified algorithm. The increased efficiency is due to the ZVS diode turn on and voltage clamping action of the diode that enables near ZVS-ZCS turn on conditions for the power MOSFET. This effect has been reported by Kazimierczuk [11] for an ideal class E amplifier. It has been demonstrated here that it also applies when a nonideal switch and finite value of supply inductance are used.

V. CONCLUSIONS

The operation of the class E amplifier including inductance in series with the switch has been expressed as a set of fifth-order state-space equations. The model was implemented in MATLAB to find the periodic solution for a given set of component values and operational parameters. The algorithm of the model also incorporates the effect of an anti-parallel diode across the switch and the nonzero switching times of a real power device. By including these effects, the model is able to provide accurate predictions of circuit performance under nonoptimal operating conditions, i.e., non-ZVS and non-ZCS.

An experimental circuit was built, using capacitor values chosen from model predictions of ZVS-ZCS operation. The simulation and experiment showed good correlation once errors due to impedance uncertainties had been nulled out.

Operation under nonoptimum conditions was investigated, and the fifth-order model was shown to agree well with experiments for both positive and negative voltages across the switch at turn on.

REFERENCES

[1] N. O. Sokal and A. D. Sokal, "Class E—a new class of high-efficiency tuned single-ended switching power amplifiers," *IEEE J. Solid-State Circuits*, vol. 10, pp. 168–176, June 1975.
[2] ——, "High-efficiency tuned switching power amplifier," U. S. Patent 3 919 656, Nov. 1975.
[3] F. H. Raab, "Idealized operation of the class E tuned power amplifier," *IEEE Trans. Circuits Syst.*, vol. 24, pp. 725–735, Dec. 1977.
[4] M. K. Kazimierczuk and K. Puczko, "Exact analysis of class-E tuned power-amplifier at any q and switch duty cycle," *IEEE Trans. Circuits Syst.*, vol. CAS-34, pp. 149–159, Feb. 1987.
[5] C. P. Avratoglou and N. C. Voulgaris, "A new method for the analysis and design of the class-E power- amplifier taking into account the $q(l)$ factor," *IEEE Trans. Circuits Syst.*, vol. CAS-34, pp. 687–691, June 1987.
[6] C.-H. Li and Y.-O. Yam, "Maximum frequency and optimum performance of class-E power-amplifiers," *Proc. Inst. Electr. Eng. Circuits Devices Syst.*, vol. 141, pp. 174–184, June 1994.
[7] J. C. Mandojana, K. J. Herman, and R. E. Zulinski, "A discrete continuous time-domain analysis of a generalized class-E amplifier," *IEEE Trans. Circuits Syst.*, vol. 37, pp. 1057–1060, Aug. 1990.
[8] C. P. Avratoglou, N. C. Voulgaris, and F. I. Ioannidou, "Analysis and design of a generalized class-E tuned power-amplifier," *IEEE Trans. Circuits Syst.*, vol. 36, pp. 1068–1079, Aug. 1989.
[9] W. H. Press, S. A. Teukolsky, W. T. Vetterling, and B. P. Flannery, *Numerical Recipes in C: The Art of Scientific Computing*. Cambridge, U.K.: Cambridge Univ. Press, 1992, pp. 742–743.
[10] M. K. Kazimierczuk and K. Puczko, "Power-output capability of class-E amplifier at any loaded-Q and switch duty cycle," *IEEE Trans. Circuits Syst.*, vol. 36, pp. 1142–1143, Aug. 1989.
[11] ——, "Class E tuned power amplifier with antiparallel diode or series diode at switch, with any loaded Q and switch duty cycle," *IEEE Trans. Circuits Syst.*, vol. 36, pp. 1201–1209, Sept. 1989.